Front. Earth Sci. 2016, 10(1): 145–158
DOI 10.1007/s11707-015-0499-2

RESEARCH ARTICLE

# Assimilation of Chinese Fengyun-3B Microwave Temperature Sounder radiances into the Global GRAPES system with an improved cloud detection threshold

**Juan LI (✉)[1,2], Guiqing LIU[1,2]**

1 Numerical Weather Prediction Center, China Meteorological Administration, Beijing 100081, China
2 National Meteorological Center, China Meteorological Administration, Beijing 100081, China



**Abstract** Fengyun-3B (FY-3B) is the second polar-orbiting satellite in the new Fengyun-three series. This paper describes the assimilation of the FY-3B Microwave Temperature Sounder (MWTS) radiances in the Chinese Numerical Weather prediction system – the Global and Regional Assimilation and PrEdiction System (GRAPES). A quality control procedure for the assimilation of the FY-3B MWTS radiance was proposed. Extensive monitoring before assimilation shows that the observations of channel 4 are notably contaminated. Channels 2 and 3 are used in this research. A cloud detection algorithm with an improved cloud-detection threshold is determined and incorporated into the impact experiments. The clear field-of-view (FOV) percentage increased from 42% to 57% with the new threshold. In addition, the newly added FOVs are located in the clear region, as demonstrated by the cloud liquid water path data from NOAA-18. The impact of the MWTS radiances on the prediction of GRAPES was researched. The observation biases of FY-3B MWTS O-B (differences between satellite observations and model simulations) significantly decreased after an empirical bias correction procedure. After assimilation, the residual biases are small. The assimilation of the FY-3B MWTS radiances shows a positive impact in the Northern Hemisphere and a neutral impact in the Southern Hemisphere.

**Keywords** Fengyun-3B (FY-3B), MWTS, quality control, GRAPES

Received May 25, 2014; accepted October 26, 2014

E-mail: lijuan@pku.org.cn

## 1 Introduction

The accuracy of Numerical Weather Prediction (NWP) has improved significantly in recent years, with satellite data among the major contributors. At present, satellite data from ATOVS (Advanced TIROS [Television and Infrared Observational Satellite] Operational Vertical Sounder), onboard NOAA (National Oceanic and Atmospheric Administration) -15, -16, -17, -18, and-19 and Aqua, has the greatest impact on forecasts produced by NWP centers (Andersson et al., 1994; Eyre, 1997; Courtier et al., 1998; Derber and Wu, 1998; English et al., 2000; McNally et al., 2000; Bouttier and Kelly, 2001; Ahn et al., 2003; Okamoto et al., 2005; Zapotocny et al., 2007). Most NWP centers, which made effective early use of ATOVS, have reported a substantial reduction in the forecast root mean square (RMS) error. Adjoint-based estimates of observation impact on NWP (Baker and Daley, 2000) have further demonstrated that the greatest decrease in forecast error is due to Advanced Microwave Sounding Unit-A (AMSU-A), which flew as a part of ATOVS and is used primarily for global atmospheric temperature sounding (Fourrié et al., 2002; Langland and Baker, 2004; Cardinali, 2009; Gelaro et al., 2010). Similar to AMSU-A, FY-3A microwave temperature radiance can also have a positive impact on NWP forecasts (Du et al., 2012; Li and Zou, 2013, 2014; Yang et al., 2013).

The second satellite of the new series of Chinese polar orbiting satellites, i.e., Fengyun-3B (FY-3B), was successfully launched on November 5, 2010 (Liu, 2011). FY-3B has an afternoon configuration. There are 11 instruments onboard the FY-3B, similar to the first satellite in the same series, the morning-configured FY-3A (Dong et al., 2009; Yang et al., 2009; Zhang et al., 2009),. The Microwave Temperature Sounder (MWTS) onboard FY-3B has four channels that are similar to AMSU-A channels 3, 5, 7, and

9 (You et al., 2012) which provide atmospheric temperature sounding.

The assimilation of microwave radiance can significantly improve the NWP forecast (Derber and Wu, 1998; Cardinali, 2009); therefore, it is important to evaluate the impact of FY-3B microwave temperature sounding observations on NWP models. Wang and Zou (2012) assess the quality of the brightness temperature measurements from FY-3B MWTS by comparing them with NWP model simulations and NOAA-18 AMSU-A measurements with the same frequencies using observations from 2011. These authors found that there is a strong latitudinal-dependent bias in both MWTS channel 3 and AMSU-A channel 7. Moreover, the brightness temperatures of channel 4 are contaminated within a small latitudinal zone (~30°−40°N) of the Northern Hemisphere. Similarly, this contamination is also indicated by Lu and Bell (2012). However, the impact of the FY-3B MWTS on NWP systems has not been evaluated.

The aim of this study was to assimilate, for the first time, FY-3B MWTS radiances into the Global and Regional Assimilation and PrEdiction System (GRAPES) (Chen et al., 2008; Xue and Chen, 2008, Xue et al., 2008). As a result, the development of observation processing and quality control (QC) for FY-3B radiances should be conducted. In 2013, a cloud detection scheme for FY-3A MWTS was proposed (Li and Zou, 2013). However, the threshold is too small, and clear pixels can be removed in the cloud detection procedures. Thus, in this research, an improved cloud detection threshold was determined for FY-3B MWTS. With this new threshold, more clear pixels will be retained.

This paper is organized as follows. Section 2 describes the general details of the FY-3B MWTS radiance data and the GRAPES three-dimensional variational assimilation (3D-Var) system. Section 3 provides a QC scheme of the FY-3B MWTS radiance data and a discussion of the first guess departures. Section 4 introduces the bias correction, the setup of the assimilation experiments, and the results of the FY-3B MWTS radiance assimilation experiments with respect to the control run. A summary and discussion are presented in Section 5.

## 2 Descriptions of the observation data and the GRAPES 3D-Var system

Level-1b radiance data from the FY-3B MWTS were employed for this study for the month of May 2013. The two-point calibration technique for AMSU-A was used to calibrate the MWTS data. Table 1 lists a few selected channel characteristics of the FY-3B MWTS, including channel frequency, peak weighting function height, and radiometric temperature sensitivity (Noise Equivalent Differential Temperature [NEDT]). The center frequencies of MWTS channels 1−4 are 50.30 GHz, (53.596±0.115) GHz, 54.94 GHz, and 57.29 GHz, respectively. MWTS channel 1 is a window channel, and channels 2−4 have weighting function peaks that are located near 700 hPa, 300 hPa, and 70 hPa, respectively. The NEDT is 0.5 K for channel 1 and 0.4 K for channels 2−4. There are 15 scene fields-of-view (FOVs) along each MWTS scan line. The horizontal FOV resolution at nadir is 62 km.

**Table 1** Channel characteristics of FY-3B MWTS

| Channel # | Center frequency /GHz | Peak weighting function height /hPa | NEDT*/K |
|---|---|---|---|
| 1 | 50.30 | surface | 0.5 |
| 2 | 53.596±0.115 | 700 | 0.4 |
| 3 | 54.94 | 300 | 0.4 |
| 4 | 57.29 | 70 | 0.4 |

*NEDT = noise equivalent temperature difference.

GRAPES-3DVar (Xue and Chen, 2008; Xue et al., 2008) is an analysis system that is designed for operational application. The 3D-Var system is carried out for four data assimilation cycles (00, 06, 12, and 18 UTC) and processes six hourly observations, which are centered at 00, 06, 12, and 18 UTC. The GRAPES-3DVar system produces an analysis through the minimization of an objective function given by

$$\begin{aligned} \boldsymbol{J}(\boldsymbol{x}) &= \boldsymbol{J}^b + \boldsymbol{J}^o \\ &= \frac{1}{2}(\boldsymbol{x}-\boldsymbol{x}^b)^{\mathrm{T}} B^{-1}(\boldsymbol{x}-\boldsymbol{x}^b) \\ &\quad + \frac{1}{2}\Big(\boldsymbol{H}(\boldsymbol{x})-\boldsymbol{y}^o\Big)^{\mathrm{T}} R^{-1}\Big(\boldsymbol{H}(\boldsymbol{x})-\boldsymbol{y}^o\Big), \end{aligned} \quad (1)$$

where $\boldsymbol{x}$ is a state vector that is composed of atmospheric and surface variables, and $\boldsymbol{x}^b$ is a background estimate of the state vector that is provided by a 6-hour forecast. $\boldsymbol{y}^o$ is a vector of all the observations. Prior to this study, the GRAPES-3DVar system could directly assimilate Radiosondes, surface synoptic observations (SYNOPs), Ship, Aircraft Report (Airep), Atmospheric Motion Vectors (AMVs), ATOVS, COSMIC RO data, etc. $\boldsymbol{H}$ is the observation operator that transforms the state vector $\boldsymbol{x}$ into observation space. For conventional observation types, this creation of a pseudo-observation requires only interpolation to the observation locations. The transformation is more complex for the radiance data. The temperature and moisture on the model grid are interpolated to the observation location to create a temperature and moisture profile. Next, a radiative transfer model is performed to generate the pseudo-observation. In the GRAPES-3DVar system, RTTOV-7 or RTTOV 9.3 (Radiative Transfer for TOVS) has been used to simulate satellite radiance (Saunders et al., 1999). RTTOV is a fast radiative transfer model in which the layer optical depth is parameterized using linear combinations of profile-dependent predictors.

Prior to this study, GRAPES 3D-Var was not able to assimilate FY-3B MWTS radiances. To do this, the fast transmittance coefficients were generated by the National Satellite Meteorological Center of CMA. The coefficients were then implemented in RTTOV to calculate the optical depths. This updated RTTOV allowed us to assimilate the FY-3B MWTS in the GRAPES system. $R$ is the estimated error covariance of the observations. The diagonals are the observation errors, and the other elements of the matrix describe the correlation between the neighboring observations. Currently, the observation errors are considered uncorrelated. $B$ is the estimated error covariance of the background field. The background covariance matrix that was used in this study was estimated using the NMC method (Parrish and Derber, 1992; Wu et al., 2002), which assumes that the background error covariances are well approximated by averaged forecast differences between 24- and 12-h forecasts verifying at the same time. The cost function assumes that observational and background error covariances are described using a Gaussian probability density function with zero mean error. The basic idea of variational assimilation is to find the closest solution to the difference between the effective observation and the background field in the given periods under the meaning of the least square method by adjusting the first guess.

The incremental analysis method is used in the GRAPES 3D-Var system (Courtier et al., 1994). The model variables include wind fields ($u$, $v$), dimensionless pressure ($\pi$), and specific humidity ($q$). The incremental cost function minimization is performed in preconditioned control variable space. The state variables are assumed to decompose balanced and unbalanced components. By introducing a simple transformation from the state variables to the control variables with a recursive or spectral filter, the convergence rate of iteration to minimize the cost function in 3DVar is greatly accelerated. The definition of dynamical balance depends on the characteristic scale of the considered circulation. The ratio of the balanced to unbalanced parts is controlled by the prescribed statistics of background error. The Limited Memory Broyden-Fletcher-Goldfarb-Shanno method is used in the GRAPES 3D-Var system (Navon and Legler, 1987).

## 3 Quality control scheme

### 3.1 Channel selection based on the FY-3B MWTS observation characteristics

MWTS channel 1 is sensitive to surface and cloud liquid water. This channel is not assimilated in the research because model simulations of brightness temperature are still inaccurate due to the uncertainty in the surface emissivity. MWTS channels 2–4 can provide the atmospheric temperature that is characteristic of the troposphere and low stratosphere.

An extensive monitoring of the FY-3B MWTS radiances is conducted before QC. The center frequencies of MWTS channels 1–4 are 50.30 GHz, (53.596±0.115) GHz, 54.94 GHz, and 57.29 GHz equivalent to the center frequencies of AMSU-A channels 3, 5, 7 and 9, respectively (Wang and Zou, 2012). The NEDT of MWTS is 0.5 K for channel 1 and 0.4 K for channels 2–4. The NEDT of the AMSU-A channels is slightly smaller than that of the MWTS channels. The NEDT of AMSU-A is 0.4 K for channel 3 and 0.25 K for channels 5, 7, and 9. Due to the similarity between the four channels of MWTS and AMSU-A channels 3, 5, 7, and 9, the NOAA-18 AMSU-A is used as a reference in assessing the performance of the FY-3B MWTS. Both FY-3B and NOAA-18 have afternoon-configured orbits (approximately 2 P.M.). The Community Radiative Transfer Model (CRTM 2.0) is used to simulate MWTS brightness temperatures (van Delst, 2011). CRTM is chosen here to make the simulation results comparable to those that were provided by Wang and Zou (2012). The 6-hour forecasts of the vertical profiles of temperature, specific humidity, and surface pressure from the National Center for Environmental Prediction (NCEP) global forecast system (GFS) are used as input to CRTM. The NCEP GFS 6-hour forecast fields have a horizontal resolution of 1°×1° and 26 vertical levels. The highest vertical level is approximately 10 hPa. Global simulations of brightness temperature are used to examine the performance of the MWTS instrument. The brightness temperature differences between the satellite observations and model simulations (O-B) are calculated. The comparisons between FY-3B MWTS channel 2 (channel 3) and NOAA18 AMSU-A channel 5 (channel 7) show similar results to those that were provided by Wang and Zou (2012). However, the results regarding channel 4 are different from those previously reported. Therefore, a comparison between FY-3B MWTS channel 4 and NOAA-18 AMSU-A channel 9 is presented and analyzed here.

Figure 1 shows a global distribution of O-B from (a) FY-3B MWTS channel 4 and (b) NOAA-18 AMSU-A channel 9 on 1 May 2013. The O-B of MWTS channel 4 shows greater global variability than that of AMSU-A channel 9. In the tropics, the O-B of MWTS channel 4 demonstrates a very large positive bias. The global mean O-B biases and standard deviations (STD) over land and ocean are shown in Fig. 2. The daily variations in the global bias and the bias over land and ocean are nearly stable for these MWTS and AMSU-A channels. For MWTS channel 4, the global bias is approximately −1.8 K. The STD is approximately 1.9 K, which is nearly four times the STD of AMSU-A channel 9.

The latitudinal dependencies of the global averaged O-B biases and standard deviations are further investigated in Fig. 3. The O-B biases and standard deviations are

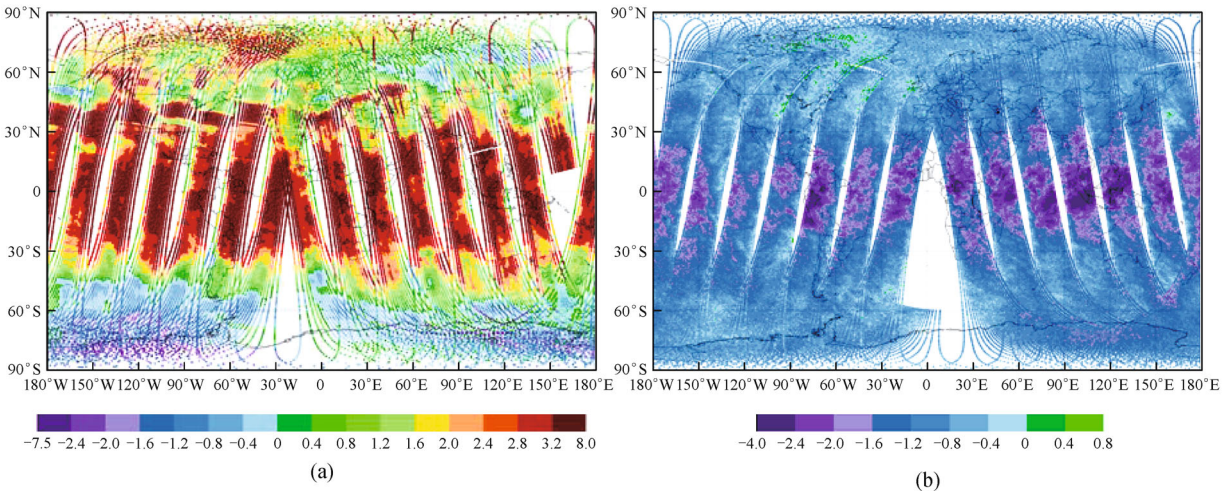


**Fig. 1** Global distribution of O-B from (a) FY-3B MWTS channel 4 and (b) NOAA-18 AMSU-A channel 9 at 0300–1500 UTC 1 May 2013.

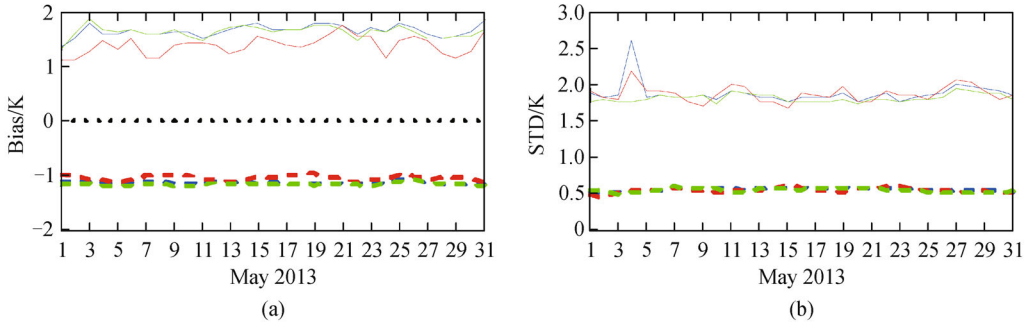


**Fig. 2** Daily variations of O-B (a) biases and (b) standard deviations of channel 4 from FY-3B MWTS (solid lines) and channel 9 from NOAA-18 AMSU-A (dashed lines) data in May 2013 over ocean (green), land (red), and both land and ocean (blue).

calculated in 18 separate latitudinal bands using data from May 2013. The O-B standard deviation of MWTS channel 4 is approximately 0.9 K in most regions, while in the high latitudes in the Southern Hemisphere, the STD can exceed 3.6 K. In contrast, the STD of AMSU-A channel 9 is generally less than 0.5 K.

Compared with the O-B biases and STDs of channel 4, calculated using observations in 2011 (Wang and Zou, 2012), the global biases of data in 2013 increased significantly from approximately 0.15 K to 1.8 K. In addition, the global STD increased from approximately 1.4 K to 1.9 K. Much more widespread distributions of contaminated observations were found in the FY-3B MWTS channel 4 radiances in 2013.

Figures 1−3 show that the instrument noises of MWTS channel 4 are much greater than those of AMSU-A channel 9. In fact, most O-B biases can be corrected in the subsequent bias correction scheme. However, a large STD will make it difficult to use the channel 4 observations. Since the correction model for the observation radiance has not yet been developed, a QC and a bias correction scheme were initially used (described later) for channel 4 data. As a result, the STD of O-B was as high as 1.5 K, and the frequency distribution of O-B was not Gaussian-like (figure omitted). Thus, channel 4 data was not used in the assimilation.

### 3.2 The cloud detection scheme with an improved threshold

Given the input profiles from the NWP models lack reliable information regarding clouds, and scattering processes cannot currently be accurately simulated in the fast radiative transfer models, the assimilation of cloud-contaminated observations will degrade the assimilation

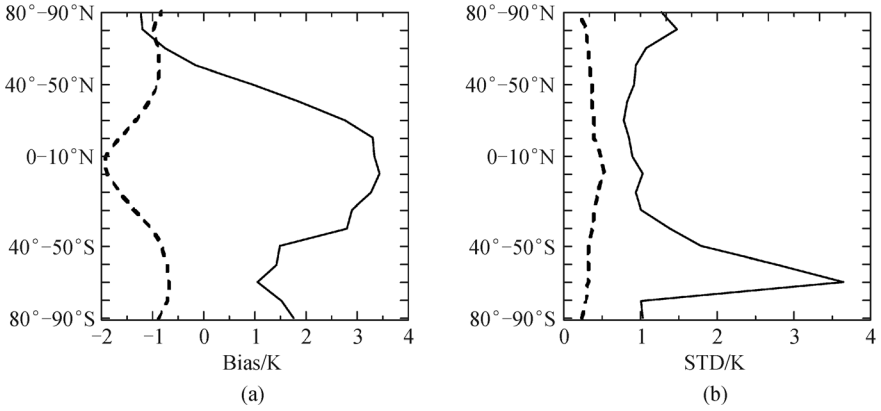


**Fig. 3** Latitudinal dependences of the global averaged O-B (a) biases and (b) STDs of channel 4 from MWTS (solid lines) and channel 9 from AMSU-A (dashed lines) data in May 2013.

system. As a result, cloud detection should be conducted. The detection scheme for the FY-3B MWTS borrows the idea that was implemented in Li and Zou (2013). In this scheme, cloud detection for MWTS is carried out using a cloud fraction product from the Visible and InfraRed Radiometer (VIRR) onboard the FY-3 series satellite. The VIRR has 10 channels spanning the spectrum from 0.455 μm to 12.5 μm, and the horizontal resolution of the pixel at nadir is 1.1 km (Dong et al., 2009, Li et al. 2009). Cloudy FOVs of VIRR are identified by a multi-threshold cloud detection method (Li and Zou, 2013). Based on these thresholds, a VIRR pixel is classified as "cloudy" or "clear" FOV. Because the spatial resolution of the MWTS is much coarser than that of the VIRR, a cloud fraction is calculated for an individual MWTS FOV. This fraction is defined by the ratio of the total number of cloudy pixels to all the VIRR pixels that are located in the MWTS FOV. An MWTS FOV with a cloud fraction that is greater than the threshold ($f_{\mathrm{VIRR}}$) 37% was identified as a cloudy scene in Li and Zou (2013).

The threshold 37% is determined by comparing the percentages of cloudy radiances as estimated from the FY-3A VIRR cloud fraction data with Meteorological Operational satellite A (MetOp-A) AMSU-A cloud percentages using one month's worth of data. The Liquid Water Path (LWP) products from the operational Microwave Surface and Precipitation Products System (MSPPS) are used for the cloud detection of AMSU-A (Weng and Grody, 1994; Ferraro et al., 2005). The LWP is only retrieved over the ocean (without sea ice) and varies from 0.01 $\mathrm{kg\cdot m^{-2}}$ to 2 $\mathrm{kg\cdot m^{-2}}$. The higher the LWP threshold is used, the more clearly the pixels will be identified. An AMSU-A FOV with an LWP greater than a threshold ($f_{\mathrm{LWP}}$) of 0.01 $\mathrm{kg\cdot m^{-2}}$ is marked as a cloudy scene in Li and Zou (2013). However, this threshold is too small based on many studies (Grody et al., 2001; QSS Group, Inc., 2005). The user guide of MSPPS (QSS Group, Inc., 2005) indicates that an AMSU-A FOV with an LWP of less than 0.05 $\mathrm{kg\cdot m^{-2}}$ is rain free. Since the wavelength of microwave channels is much longer than that of infrared channels, the upward radiance will not be contaminated by cloud or rain with an LWP of less than 0.05 $\mathrm{kg\cdot m^{-2}}$. In 2011, Zou et al. (2011) used the threshold of 0.05 $\mathrm{kg\cdot m^{-2}}$ to detect AMSU-A cloud-contaminated FOVs. The outliers are removed efficiently with this threshold. Therefore, the AMSU-A FOVs with an LWP of equal to or less than 0.05 $\mathrm{kg\cdot m^{-2}}$ can be regarded as clear pixels. These thresholds can be used to identify the FY-3B VIRR cloud fraction threshold. However, if 0.05 $\mathrm{kg\cdot m^{-2}}$ is chosen as the threshold, the corresponding threshold $f_{\mathrm{VIRR}}$ will be approximately 100%. Similarly, if the threshold is set at 0.04 $\mathrm{kg\cdot m^{-2}}$, the $f_{\mathrm{VIRR}}$ is approximately 94%. In this situation, only FOVs that are almost entirely covered by clouds are removed. To ensure that no cloudy radiance will be assimilated in the subsequent experiments in this study, a more stringent threshold of 0.03 $\mathrm{kg\cdot m^{-2}}$ was used to identify the cloudy FOVs for AMSU-A.

Figure 4(a) displays the global percentage number of MWTS FOVs, with a cloud fraction greater than $f_{\mathrm{VIRR}}$, and NOAA-18 AMSU-A FOVs, with the LWP greater than $f_{\mathrm{LWP}}$, for data from May 2013. The cloudy FOV percentage decreases with the increasing threshold. When the $f_{\mathrm{LWP}}$ is set to 0.03 $\mathrm{kg\cdot m^{-2}}$, the cloudy FOV percentage is approximately 42% (Fig. 4(b)). Similarly, when $f_{\mathrm{VIRR}}$ equals 76%, the cloud coverage is approximately 42% over the ocean, which is almost equivalent to the cloud percentage of AMSU-A. The value of 76% is thus chosen as the new threshold instead of the old one of 37%. The cloudy FOV percentage decreases approximately 15% when using the threshold. The increased threshold will allow for more clear pixels to pass the quality control.

Figure 5 shows the distribution of the MWTS clear pixels that were identified by cloud fractions that were smaller than 37% (green dots) or between 37% and 76% (red dots) over the ocean. NOAA-18 AMSU-A FOVs with an LWP less than 0.03 $\mathrm{kg\cdot m^{-2}}$ are displayed in gray dots. The FOVs at the scan edge are displayed in black dots to show the AMSU-A scan swath gaps. Both green and red

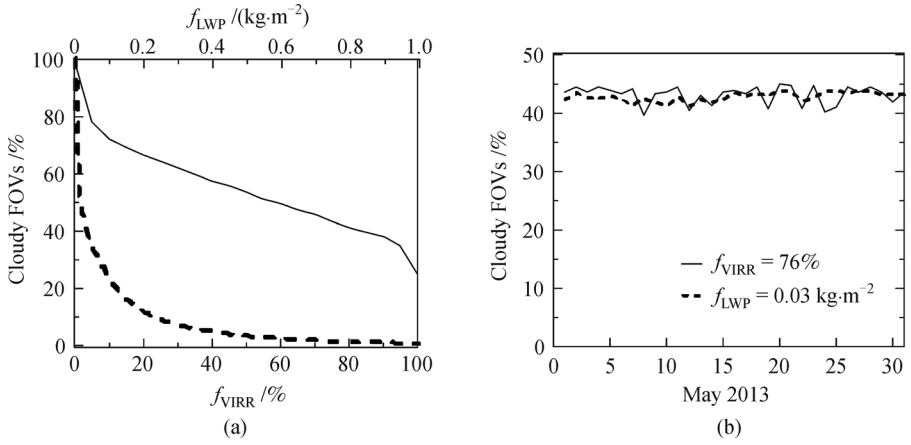


**Fig. 4** (a) Global percentage number of MWTS FOVs (solid line), with the cloud fraction greater than $f_{VIRR}$, and NOAA-18 AMSU-A FOVs (dashed line), with the LWP greater than $f_{LWP}$ for data in May 2013. (b) Daily variations of cloudy MWTS FOV number percentages when $f_{VIRR}$ is 76% (solid line) and cloudy AMSU-A FOV number percentages when $f_{LWP}$ is 0.03 kg·m$^{-2}$ (dashed line).

dots are observations that have passed the cloud detection scheme for the FY-3B MWTS in this research. The green dots are the pixels that were identified by the old threshold. As shown in the illustration, the newly added FOVs (red dots) are also located in the clear region as demonstrated by AMSU-A LWP retrievals. With the new threshold, more clear pixels will be retained after the cloud-detection procedures.

The bias and standard deviation of O-B from the MWTS clear pixels that were identified by the cloud fraction of less than 37% or 76% during May 2013 are displayed in Fig. 6. The bias of O-B from channel 2 or channel 3 data is almost unchanged after adding more clear pixels, indicating that the newly added observations have similar bias characteristics as those that were identified by the cloud fraction of less than 37%. In addition, the STDs of O-B from the clear pixels slightly decreased after using the new threshold of 76%. With the new threshold of 76%, we can obtain more clear observations. Due to the definition of STD, additional samples will decrease it. Therefore, a lower STD comes with more clear observations, and the STD of O-B from clear pixels, as identified by the cloud fraction of 76%, is smaller than that identified by the cloud fraction of 37%.

### 3.3 Other quality control procedures

The two outmost FOVs (i.e., FOV 1, 2, 14, and 15), channel 2 FOVs that are over sea ice and land, channel 3 FOVs that are over a terrain altitude higher than 500 m, and coastal FOVs are removed. In addition, cloudy FOVs are detected with cloud fractions greater than 76%.

After the previous QC procedures, a biweighting quality control procedure is applied to identify outliers. The outliers are defined as those measurements with values that deviate from the model-simulated values by more than Z-score times the STD (Lansante, 1996; Zou and Zeng, 2006). First, the biweight mean ($\mu_{bm}$) and the biweight STD ($\sigma_{bsd}$) of the following variables are calculated (Lansante, 1996; Zou and Zeng, 2006):

$$x = \frac{\Delta T_b}{T_b^{bg}} = \frac{T_b^{obs} - T_b^{bg}}{T_b^{bg}}, \tag{2}$$

where $T_b^{obs}$ and $T_b^{bg}$ represent the observed and model-simulated brightness temperature, respectively. Here, the biweight mean and biweight STD are similar to the traditional mean and STD except that the impact of outliers to their values is minimized. Then, a $Z$-score for all of the data that pass all of the checks for cloud, terrain height, and surface type is calculated:

$$Z_i = \frac{x_i - \mu_{bm}}{\sigma_{bsd}}, \tag{3}$$

where the subscript "$i$" indicates the $i^{th}$ datum. Data with a $Z$-score of more than two are removed. Considering the variations of the mean states of the atmosphere at different latitudes, the biweighting quality control is implemented separately in three separate latitudinal bands: tropics (30°N −30°S), middle latitudes (30°N−60°N, 30°S−60°S), and high latitudes (60°N−90°N, 60°S−90°S).

## 4 Assimilation results

### 4.1 Experimental setup

Two different experiments were conducted from May 1 to May 31, 2013. The control run (CTRL) assimilates conventional observations, NOAA-15/18 AMSU-A, MetOp-A AMSU-A, and COSMIC RO observations. The conventional observations contain a global set of surface and upper-air reports, including Radiosondes,

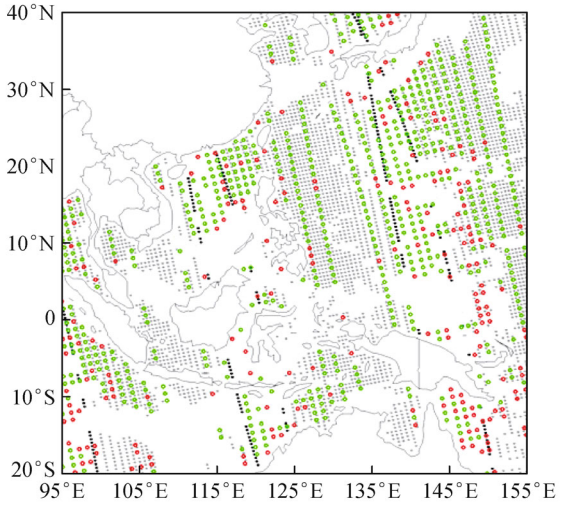


**Fig. 5** Distribution of the MWTS clear pixels identified by cloud fraction less than 37% (green dots), between 37% and 76% (red dots) over the ocean during the period from 0300UTC to 0900UTC, May 30, 2013. NOAA-18 AMSU-A FOVs with LWP less than 0.03 $kg \cdot m^{-2}$ are shown in grey dots (the FOVs at the scan edge of AMSU-A are in black).

SYNOP, Ship, Airep, and AMVs from the Global Telecommunications System (GTS). The setup for the experimental (EXP) run is identical to the control run except that the FY-3B MWTS radiances are used. The observational errors for the FY-3B MWTS are set to the Noise Equivalent Temperature (NEDT) of FY-3B MWTS channels. The NEDT is shown in Table 1.

### 4.2 Analysis/forecast cycle experiments

The quality control procedures that were described in Section 3 are implemented in the EXP experiment. Figure 7 shows the distribution of the MWTS outliers that were identified by land, coastal FOVs, sea ice, scan edge, terrain altitude greater than 500 m, cloud detection, and O-B biweighting check, as well as the remaining data on 0300 UTC−0900 UTC May 30, 2013. Only clear observations over ocean are retained for channel 2. Some channel 3 radiance data over land with a low terrain altitude remain. These data can contribute to the NWP analysis and forecast over land. The biweighting quality control procedures remove some residual cloudy FOVs that have passed the cloud detection scheme. As indicated in Fig. 7(a), the observations that are removed by the biweighting check are typically located near cloudy FOVs. These outliers are probably associated with those observations that are affected by clouds and precipitation. These outliers cannot be simulated from the radiative transfer model because the input profiles from the NWP models lack reliable information in regard to clouds.

Figure 8 displays the scatter distributions of brightness temperature biases for the MWTS channel 2 and channel 3 from 1−5 May 2013 against the simulated brightness temperatures. The O-B differences of the outliers and their variations are much larger than those of the remaining data. The differences between the MWTS observations and model simulations for channel 2 can exceed ±5 K (Fig. 8 (a)). However, the measurements of channel 3 compare much more favorably with the model simulations because they are not as sensitive to the sophisticated surface characteristics. After the QC, the biases vary within a smaller range for the two channels, and the O-B differences do not show obvious temperature dependency.

On average, approximately 24% and 35% of the observations remain for channel 2 and channel 3, respectively (Fig. 9(a)). Additional outliers are identified for channel 2 because it is a lower-level sounding channel. The monthly mean global biases and standard deviations of brightness temperature differences between satellite observations and model simulations are shown in Figs. 9(b) and 9(c), both with and without removing the outliers. Channel 3 has greater biases and STD than channel 2 before QC. Both of these channels have negative biases. After QC, the STD of both channels are reduced. The STDs of channel 2 and channel 3 are approximately 0.24 K and 0.32 K, respectively. Channel 3 slightly increases in regard to the biases. A possible reason for the increased biases of channel 3 is that the random errors (as described in Fig. 9(c)) are reduced after QC, after which systematic error is more obvious. The remaining biases are approximately −1.1 K and −1.7 K for channel 2 and channel 3,

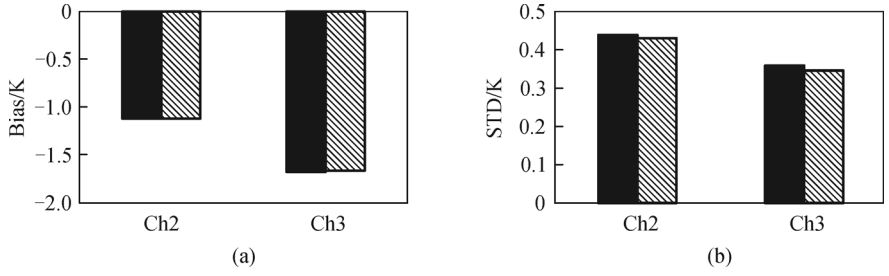


**Fig. 6** (a) Bias and (b) STD of brightness temperature differences between observations and model simulations from MWTS clear pixels identified by cloud fraction less than 37% (solid bars) or 76% (dashed bars) over the ocean during May 2013.

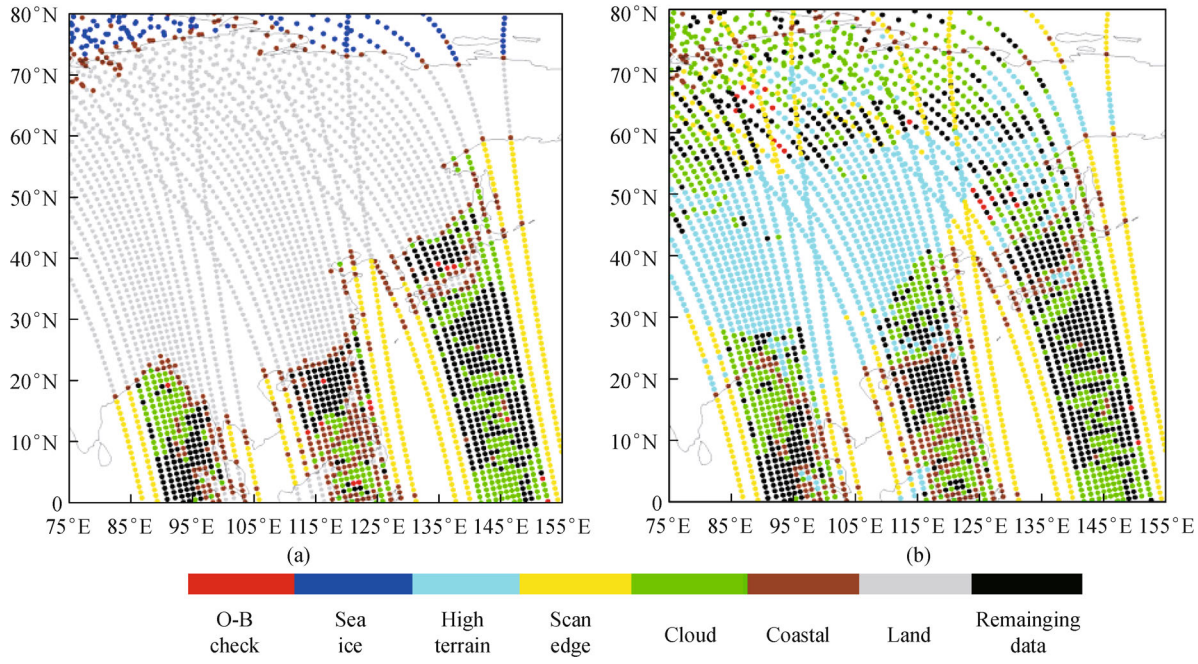


**Fig. 7** Distribution of the MWTS (a) channel 2 and (b) channel 3 outliers identified by land, coastal FOVs, sea ice, scan edge, terrain altitude greater than 500 m, cloud detection, and O-B biweighting check, as well as the remaining data on 0300 UTC−0900 UTC May 30, 2013.

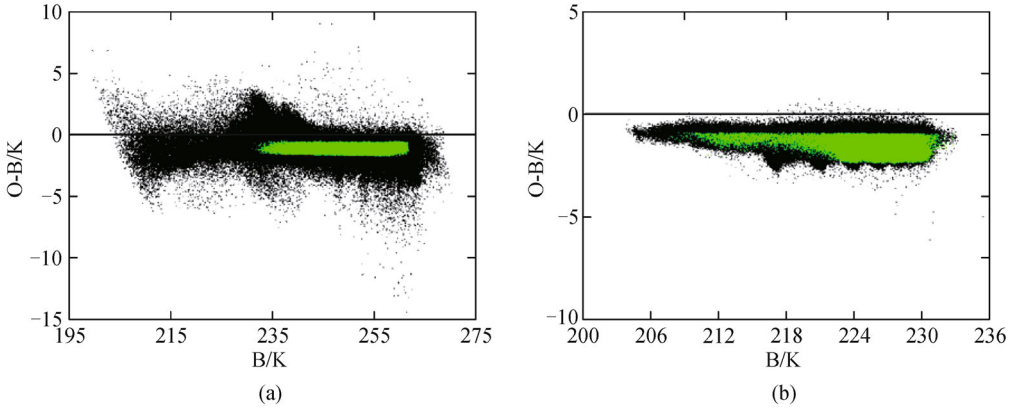


**Fig. 8** Scatter plots of O-B vs. brightness temperature for the MWTS (a) channel 2 and (b) channel 3 outliers (black) and remaining data (green) during 1−5 May 2013.

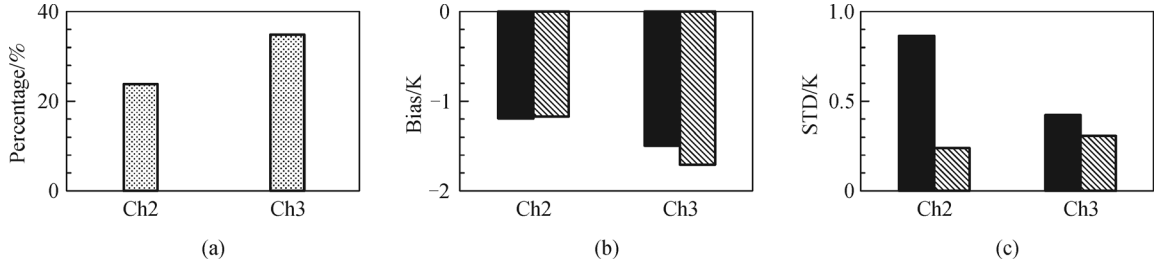


**Fig. 9** (a) Percentages of the MWTS data that passed QC in May 2013; (b) global biases; and (c) standard deviations of brightness temperature differences between observations and model simulations before (solid bars) and after (dashed bars) quality control in May 2013.

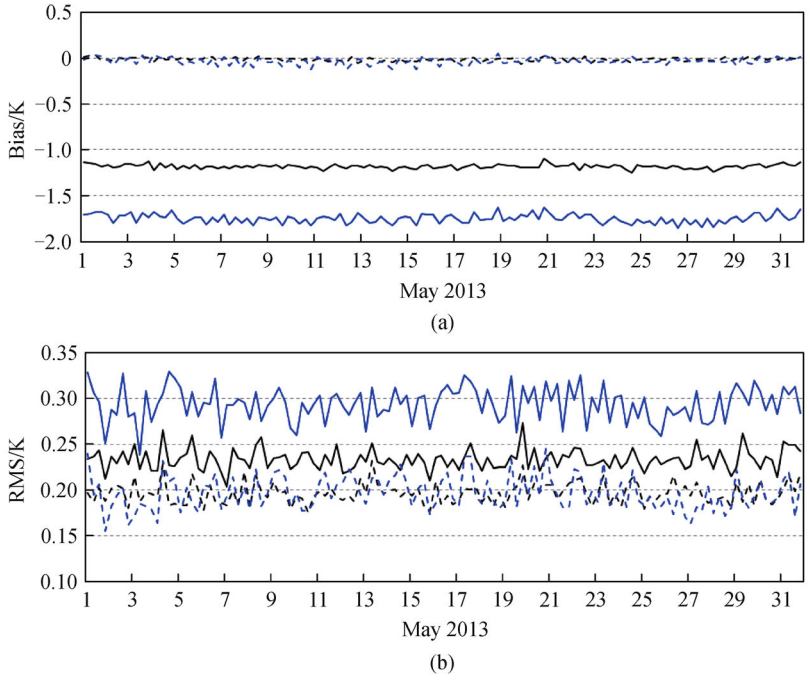


**Fig. 10** Daily variations of global (a) mean bias and (b) RMS of O-B for MWTS channels 2 (black) and channel 3 (blue) before (solid lines) and after (dashed lines) bias correction during May 2013.

respectively. These biases will be removed by the subsequent bias-correction procedures.

Data assimilation schemes assume unbiased O-B. However, the bias between observed and first-guess radiances always exists due to the inaccuracies in RTTOV, the error in the calibration of the satellite instrument, and the error in the first-guess model profiles of temperature and humidity. To assimilate the FY-3B MWTS radiances, bias correction is an essential step. The biases are calculated using an empiric bias-correction method that is provided by Harris and Kelly (Harris and Kelly, 2001; Liu et al., 2007). The biases are then subtracted from the FY-3B MWTS observed radiance. Figure 10 shows the daily variation of global mean bias and RMS of O-B for MWTS channels before and after bias correction. The biases and root mean squares of O-B are significantly reduced. In most cases, the averaged biases after the bias correction are within ±0.1 K. Figure 11 displays the distribution of O-B and O-A (brightness temperature difference between observation and analysis) for channels 2−3 in EXP. After the analysis, the O-A is obviously smaller than the O-B. In most cases, the O-A is within ±0.2 K. Therefore, the minimization is efficient, and the MWTS observation radiances impact the analysis.

MWTS channels 2 and 3 measure the thermal radiation from the troposphere. The weighting function of channel 2 (channel 3) peaks near 700 hPa (300 hPa). That is, the MWTS observed radiance of channel 2 (channel 3) is primarily from the level of 700 hPa (300 hPa). The influences of these observations on the temperature analysis field are analyzed. Figure 12 presents the analysis temperature difference on model level 10 (approximately 700 hPa) and model level 19 (approximately 300 hPa) between the EXP and CTRL experiments when assimilating only MWTS channel 2, only channel 3, or both channel 2 and channel 3 in EXP at 0600UTC on May 30, 2013. The differences between CTRL and EXP mostly appear in the region where the residual biases (O-A) of FY-3B MWTS are significantly smaller than the innovation (O-B) as presented Fig. 11. Because the observed radiance of MWTS channel 2 is primarily from the level of 700 hPa, the impact on the 3D-Var system is mainly on this level. As shown in Fig. 12(a), the analysis temperature difference between EXP and CTRL experiments on the level of 700 hPa is more significant than that on the level of 300 hPa (as shown in Fig. 12(b)). For experiments assimilating only MWTS channel 3, the result is similar to that of channel 2. Under the impact of the vertical correlation structure of the background error covariance, the assimilation of channel 3 (weighting function peaks at 300 hPa) affects the temperature field on the level of 700 hPa (shown in Fig. 12(e)). Therefore, Figure 13(e) is different from Fig. 13(a). Similarly, the assimilation of channel 2 (weighting function peaks at 700 hPa) also affects the temperature field on the level of 300 hPa (as shown in Fig. 12(f)).

The analysis field of CTRL and EXP is verified against that of the NCEP analysis. Figure 13 shows the RMS and bias of geopotential height from the analysis field and the 6-hour forecast difference between CTRL and NCEP, and EXP and NCEP in the Northern and Southern Hemi-

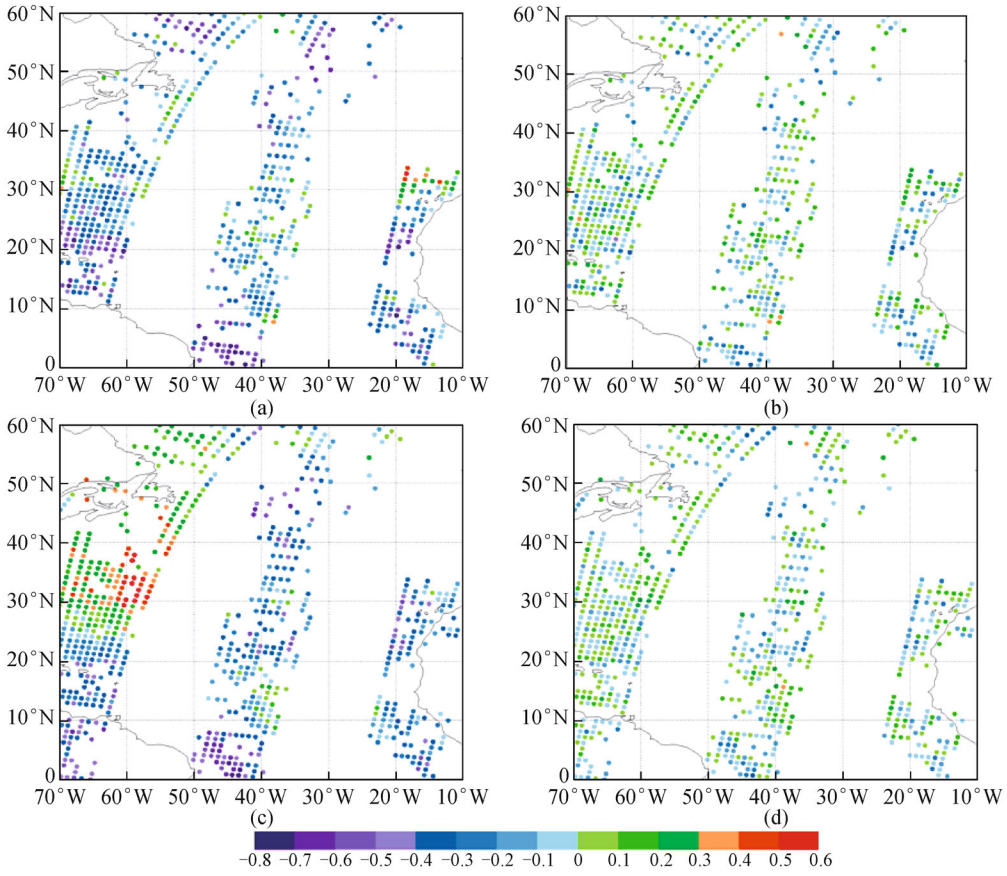


**Fig. 11** Distribution of O-B (left panels) and O-A (right panels) for MWTS (a)−(b) channel 2 and (c)−(d) channel 3 on 0300UTC−0900 UTC May 30, 2013.

spheres from 1−31 May 2013. The figures indicate that the biases and root mean squares of the analysis field are smaller than those of the 6-hour forecast. In addition, the impact of assimilation is positive in the Northern Hemisphere. As expected, the maximum impact of the FY-3B MWTS radiances is observed in the mid-upper level field (approximately 500 hPa). With the assimilation of FY-3B radiances, the geopotential height RMS of the upper level is significantly decreased. The impact on the mid-upper level analysis field will also influence the low-level field when the forecasts are conducted. In addition, the impact of FY-3B MWTS radiances on the geopotential height is neutral, with the two lines almost overlapping in the Southern Hemisphere. The results of the impact on the temperature field are similar to those on the geopotential height field.

Finally, the forecasts are verified against their own analyses. An overall measurement of the quality of medium-range forecasts for predicting a large-scale weather system is widely given by the anomaly correlation coefficient (ACC) of a 500-hPa-height forecast field. The ACC is defined as follows:

$$\mathrm{ACC} = \frac{\sum (F - C - M_{fc})(A_v - C - M_{vc})}{[\sum (F - C - M_{fc})^2 \sum (A_v - C - M_{vc})^2]^{\frac{1}{2}}}, \quad (4)$$

$$M_{fc} = \frac{1}{N} \sum (F - C), \quad (5)$$

$$M_{vc} = \frac{1}{N} \sum (A_v - C), \quad (6)$$

where $F$ is the forecast, $A_v$ is the analysis, $C$ is the climatological mean, and $N$ is the grid number in the verification region.

A key performance indicator for the forecast system is the forecast range at which the ACC decreases to 60%. Seven-day forecasts were produced for each day of the one-month period in this study. The average 500-hPa ACC and RMS errors are shown in Fig. 14 for both of the hemispheres. In the Northern Hemisphere, a small ACC difference could be observed after day 3 in the EXP. In addition, the RMS of EXP is slightly smaller than the CTRL. The Northern Hemisphere results are slightly

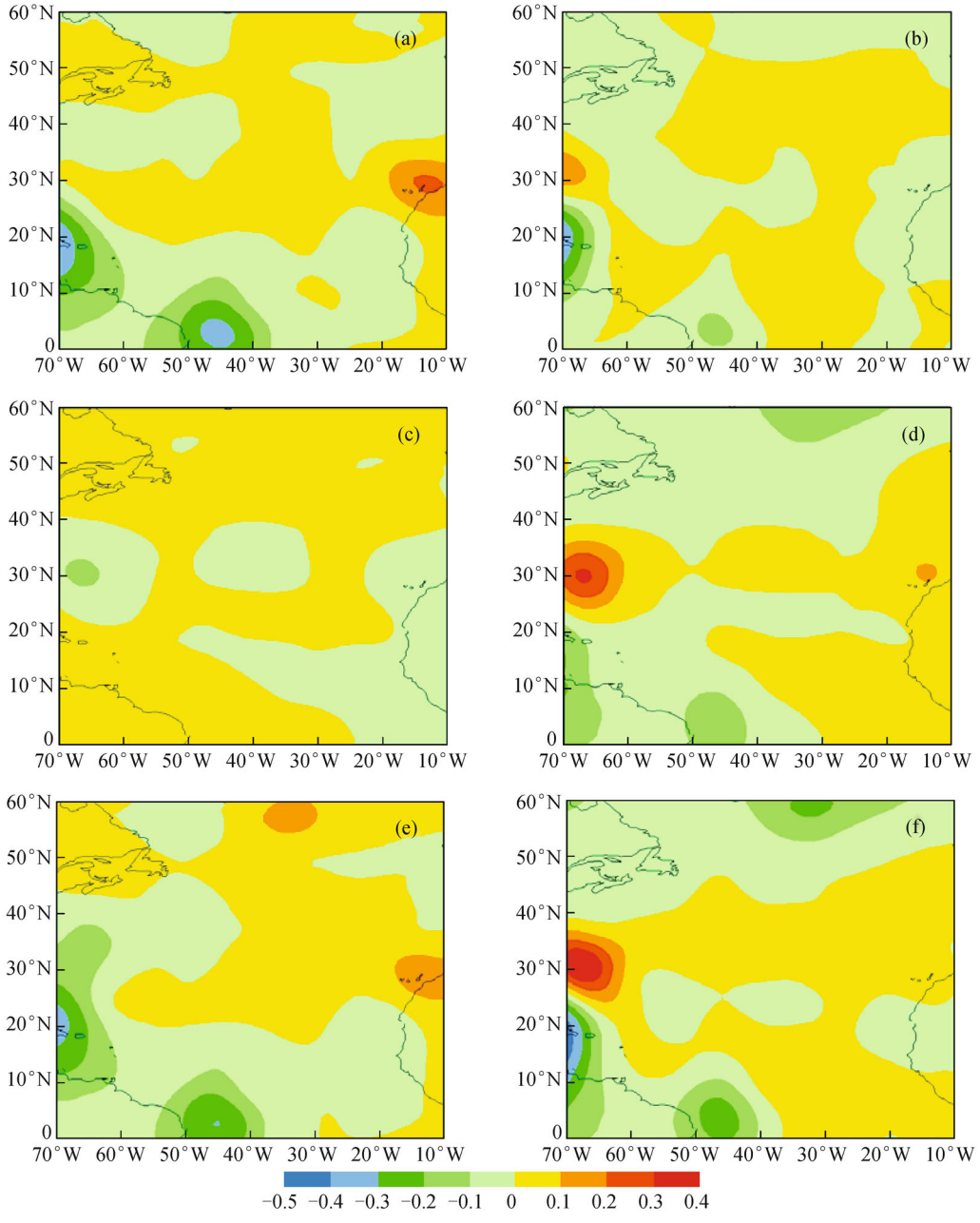


**Fig. 12** Analysis temperature difference (contour, K) on model level 10 (about 700 hPa; left panels) and model level 19 (about 300 hPa; right panels) between EXP and CTRL experiments when assimilating only MWTS (a)−(b) channel 2, (c)−(d) only channel 3, (e)−(f) both channel 2 and channel 3 in EXP at 0600UTC on May 30, 2013.

improved when using the FY-3B MWTS radiance later in the forecast. In the Southern Hemisphere, the improvement is almost neutral. In general, a neutral to small positive impact of FY-3B MWTS is found in the experiments.

## 5 Summary and discussion

In this research, the assimilation of the FY-3B MWTS radiances in the Chinese NWP system-Global GRAPES system was conducted. QC schemes for FY-3B MWTS were proposed and applied in the GRAPES system. The channel selection scheme was put forward based on the characteristics of the FY-3B MWTS observations. The radiance data of channel 4 were not used in this study according to the monitoring results. A cloud-detection algorithm with an improved cloud-detection threshold was incorporated based on the cloud fraction product that is

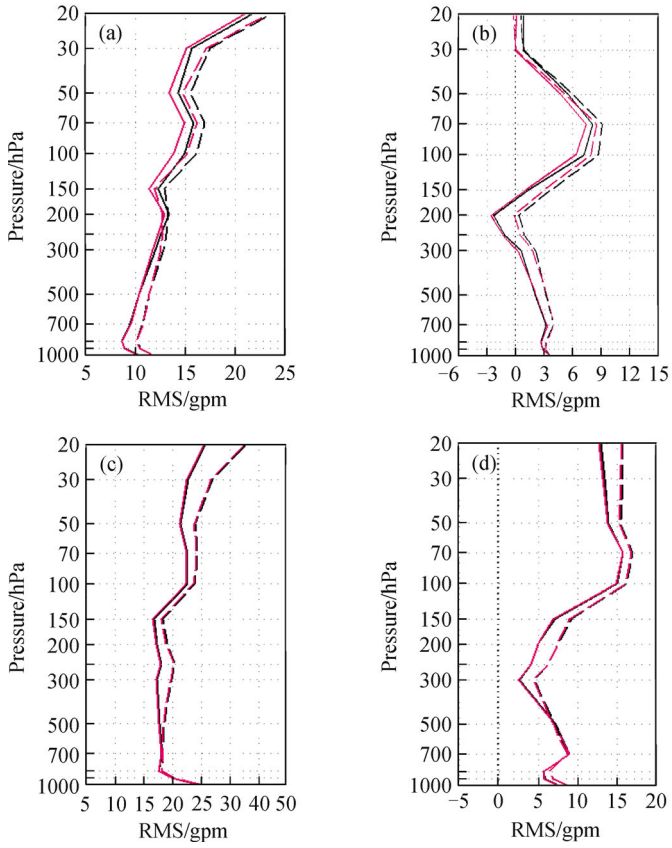


**Fig. 13** (a) RMS of geopotential height from the analysis field (solid lines) and 6-hour forecast (dashed lines) difference between CTRL and NCEP (black), and EXP and NCEP (red) in the Northern Hemisphere from 1−31 May 2013. (b) Similar to (a) but for the bias of geopotential height. (c) Similar to (a) but for the Southern hemisphere. (d) Similar to (c) but for the bias of geopotential height.

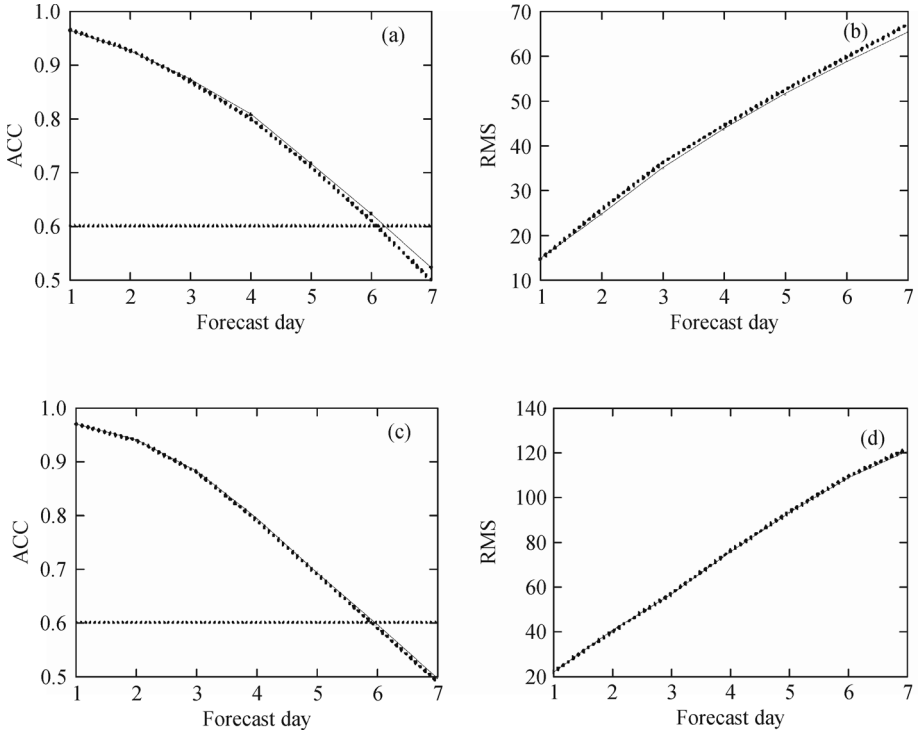


**Fig. 14** Mean ACC (left panels) and RMS (right panels) of 500 hPa geopotential height of CTRL (dashed line) and EXP (solid line) experiments in (a−b) the Northern and (c−d) the Southern Hemispheres for the period from 1−31 May 2013.

provided by the VIRR onboard FY-3B. The newly added pixels were also clear when comparing them with the NOAA-18 LWP retrievals. The clear FOVs percentage increased from 42% to 57% with the new threshold. After adding new pixels, the bias of the O-B of channel 2 or channel 3 was almost unchanged, and the standard deviation of O-B slightly decreased. The application of the improved cloud-detection threshold could maintain more clear pixels than those that were used in FY-3A MWTS. Other QC steps are based on the underlying surface characteristics and the differences between model simulations and observations. The biweighting QC can remove some residual cloudy FOVs that have passed the cloud-detection scheme. Approximately 76% and 65% of the MWTS observations were removed by the proposed QC for channels 2−3, respectively. After QC, the standard deviation of O-B decreased significantly from 0.86 K to 0.24 K for channel 2 and from 0.43 K to 0.32 K for channel 3.

The impact of the MWTS radiances on the prediction of GRAPES was studied. In the assimilation, the biases were corrected efficiently. The assimilation produces a small residual bias. The differences between CTRL and EXP mostly appear in the region where the residual biases (O-A) of FY-3B MWTS are significantly smaller than the innovation (O-B). In the experiment that only assimilated MWTS channel 2, the impact was primarily on the peak weighting function height level (700 hPa). The results of channel 3 are similar to those of channel 2. The assimilation of the MWTS could bring a neutral to small positive impact to the assimilation and model forecast. Compared to the NCEP analysis, the assimilation of the FY-3B MWTS channel 2 and channel 3 radiances shows a positive impact on the mid-upper tropospheric geopotential height in the Northern Hemisphere and a neutral impact in the Southern Hemisphere. Analysis/forecast cycle experiments were conducted for a month. Verifications indicate that the ACC of the 500-hPa-height forecast field slightly increased and that the RMS slightly decreased in the Northern Hemisphere. In all, the use of FY-3B MWTS can have a neutral to small positive impact on model forecast.

This study demonstrates the impact of the FY-3B MWTS observations on a NWP system and the application of a QC scheme. FY-3A and FY-3B are morning-orbit and afternoon-orbit satellites, respectively. The similarities and differences between the two satellites will be further explored. In addition, the Chinese FY-3C satellite was launched successfully into an afternoon-orbit on 23 September 2013; the potential value of the MWTS-II and the Microwave Humidity and Temperature Sounder (MWHTS) onboard FY-3C will also be investigated further.

**Acknowledgements** This work was jointly supported by the China Special Fund for Meteorological Research in the Public Interest (No. GYHY201106008 and No. GYHY201406008), project supported by the National Natural Science Foundation of China (Grant Nos. 91337218, 41475103, and 41375013). The authors would like to acknowledge Prof. Qifeng Lu and Prof. Gang Ma for providing the new regression coefficients for the transmittance parameterization in the fast RTM and the FY-3B MWTS radiance data.

## References

Ahn M H, Kim M J, Chung C Y, Suh A S (2003). Operational implementation of the ATOVS processing procedure in KMA and its validation. Adv Atmos Sci, 20(3): 398–414

Andersson E, Pailleux J, Thepaut J N, Eyre J R, McNally A P, Kelly G A, Courtier P (1994). Use of cloud-cleared radiances in three-four-dimensional variational data assimilation. Q J R Meteorol Soc, 120 (517): 627–653

Baker N L, Daley R (2000). Observation and background adjoint sensitivity in the adaptive observation-targeting problem. Q J R Meteorol Soc, 126(565): 1431–1454

Bouttier F, Kelly G (2001). Observing-system experiments in the ECMWF 4D-Var data assimilation system. Q J R Meteorol Soc, 127 (574): 1469–1488

Cardinali C (2009). Monitoring observation impact on short-range forecast. Q J R Meteorol Soc, 135(638): 239–250

Chen D H, Xue J S, Yang X S, Zhang H L, Shen X S, Hu J L, Wang Y, Ji L R, Chen J B (2008). New generation of multi-scale NWP system (GRAPES): general scientific design. Chin Sci Bull, 53(22): 3433–3445

Courtier P, Thépaut J N, Hollingsworth A (1994). A strategy for operational implementation of 4D-Var using an incremental approach. Q J R Meteorol Soc, 120(519): 1367–1387

Courtier P, Andersson E, Heckley W, Vasiljevic D, Hamrud M, Hollingsworth A, Rabier F, Fisher M, Pailleux J (1998). The ECMWF implementation of three-dimensional variational assimilation (3D-Var). I: formulation. Q J R Meteorol Soc, 124: 1783–1807

Derber J C, Wu W S (1998). The use of TOVS cloud-cleared radiances in the NCEP SSI analysis system. Mon Weather Rev, 126(8): 2287–2299

Dong C H, Yang J, Yang Z D, Lu N M, Shi J M, Zhang P, Liu Y J, Cai B, Zhang W (2009). An overview of a new Chinese weather satellite FY-3A. Bull Am Meteorol Soc, 90(10): 1531–1544

Du M B, Yang Y M, Yang Y H, Zhang J, Zhu X (2012). Bias correction for FY-3A microwave sounding data with its application to typhoon track forecast. Journal of Applied Meteorological Science, 23(1): 89–95 (in Chinese)

English S J, Renshaw R J, Dibben P C, Smith A J, Rayer P J, Poulsen C, Saunders F W, Eyre J R (2000). A comparison of the impact of TOVS and ATOVS satellite sounding data on the accuracy of numerical weather forecasts. Q J R Meteorol Soc, 126(569): 2911–2931

Eyre J R (1997). Variational assimilation of remotely-sensed observations of the atmosphere. J Meteorol Soc Jpn, 75(1b): 331–338

Ferraro R R, Weng F Z, Grody N C, Zhao L M, Meng H, Kongoli C, Pellegrino P, Qiu S, Dean C (2005). NOAA operational hydrological products derived from the advanced microwave sounding unit. IEEE Trans Geosci Rem Sens, 43(5): 1036–1049

Fourrié N, Doerenbecher A, Bergot T, Joly A (2002). Adjoint sensitivity of the forecast to TOVS observations. Q J R Meteorol Soc, 128(586): 2759–2777

Gelaro R, Langland R H, Pellerin S, Todling R (2010). The THORPEX observation impact intercomparison experiment. Mon Weather Rev, 138(11): 4009–4025

Grody N, Zhao J, Ferraro R, Weng F, Boers R (2001). Determination of precipitable water and cloud liquid water over oceans from the NOAA 15 advanced microwave sounding unit. Journal of Geophysical Research: Atmospheres (1984–2012), 106(D3): 2943–2953

Harris B A, Kelly G (2001). A satellite radiance-bias correction scheme for data assimilation. Q J R Meteorol Soc, 127(574): 1453–1468

Langland R H, Baker A L (2004). Estimation of observation impact using the NRL atmospheric variational data assimilation adjoint system. Tellus, Ser A, Dyn Meterol Oceanogr, 56(3): 189–201

Lansante J R (1996). Resistant, robust and non-parametric techniques for the analysis of climate data: theory and examples, including applications to historical radiosonde station data. Int J Climatol, 16 (11): 1197–1226

Li J, Zou X (2013). A quality control procedure for FY-3A MWTS measurements with emphasis on cloud detection using VIRR cloud fraction. J Atmos Ocean Technol, 30(8): 1704–1715

Li J, Zou X (2014). Impact of FY-3A MWTS radiances on prediction in GRAPES with comparison of two quality control schemes. Front Earth Sci, 8(2): 251–263

Li Y, Rong Z, Zheng Z, Liu J, Zhang L, Zhang L, Hu X, Zhang Y, Sun L (2009). Post launch site calibration of visible and near-infrared channels of FY-3A visible and infrared radiometers. Optics and precision engineering, 17(12): 2966–2974

Liu R (2011). FY-3B Satellite Delivered to CMA. Aerospace China, 2: 10

Liu Z Q, Zhang F Y, Wu X B, Xue J S (2007). A regional ATOVS radiance-bias correction scheme for radiance assimilation. Acta Meteorologica Sinica, 65(1): 113–123 (in Chinese)

Lu Q, Bell W (2012). Evaluation of FY-3B data and an assessment of passband shifts in AMSU-A and MSU during the period 1978–2012. Interim report of Visiting Scientist mission NWP_11_05, Document NWPSAF-EC-VS-023, Version 0.1, 28

McNally A P, Derber J C, Wu W, Katz B B (2000). The use of TOVS level-1b radiances in the NCEP SSI analysis system. Q J R Meteorol Soc, 126(563): 689–724

Navon I M, Legler D M (1987). Conjugate gradient methods for large scale minimization in meteorology. Mon Weather Rev, 115(8): 1479–1502

Okamoto K, Kazumori M, Owada H (2005). The assimilation of ATOVS radiances in the JMA global analysis system. J Meteorol Soc Jpn, 83 (2): 201–217

Parrish D F, Derber J C (1992). The National Meteorological Centers spectral statistical interpolation analysis system. Mon Weather Rev, 120(8): 1747–1763

QSS Group, Inc. (2005). Microwave Surface and Precipitation Products System (MSPPS) Users' Manual (UM). NOAA, NESDIS. 28–29

Saunders R W, Matricardi M, Brunel P (1999). An improved fast radiative transfer model for assimilation of satellite radiance observations. Q J R Meteorol Soc, 125(556): 1407–1425

Van Delst P (2011). CRTM: v2.0 User Guide. Joint Center for Satellite Data Assimilation, Camp Springs, Maryland, USA

Wang X, Zou X (2012). Quality assessments of Chinese FengYun-3B Microwave Temperature Sounder (MWTS) measurements. IEEE Trans Geosci Rem Sens, 50(12): 4875–4884

Weng F, Grody N C (1994). Retrieval of cloud liquid water using the special sensor microwave imager (SSM/I). J Geophys Res, 99(D12): 25535–25551

Wu W S, Purser R J, Parrish D F (2002). Three-dimensional variational analysis with spatially inhomogeneous covariances. Mon Weather Rev, 130(12): 2905–2916

Xue J S, Chen D H (2008). Numerical Prediction System Design and Application of Science GRAPES. Beijing: Science Press (in Chinese)

Xue J S, Zhuang S Y, Zhu G F, Zhang H, Liu Z Q, Liu Y, Zhuang Z R (2008). Scientific design and preliminary results of three-dimensional variational data assimilation system of GRAPES. Chin Sci Bull, 53 (22): 3446–3457

Yang J, Dong C H, Lu N M, Yang Z D, Shi J M, Zhang P, Liu Y J, Cai B (2009). FY-3A: the new generation polar-orbiting meteorological satellite of China. Acta Meteorologica Sinica, 67(4): 501–509 (in Chinese)

Yang Y M, Du M B, Zhang J (2013). FY-3A satellite microwave data assimilation experiments in tropical cyclone forecast. Journal of Tropical Meteorology, 19(3): 297–304 (in Chinese)

You R, Gu S Y, Guo Y, Wu X B, Yang H, Chen W X (2012). Long-term calibration and accuracy assessment of the FengYun-3 microwave temperature sounder radiance measurements. IEEE Trans Geosci Rem Sens, 50(12): 4854–4859

Zapotocny T H, Jung J A, Le Marshall J F, Treadon R E (2007). A two-season impact study of satellite and in situ data in the NCEP global data assimilation system. Weather Forecast, 22(4): 887–909

Zhang P, Yang J, Dong C H, Lu N M, Yang Z D, Shi J M (2009). General introduction on payloads, ground segment and data application of Fengyun 3A. Front Earth Sci, 3(3): 367–373

Zou X, Wang X, Weng F, Guan L (2011). Assessments of Chinese FengYun Microwave Temperature Sounder (MWTS) measurements for weather and climate applications. J Atmos Ocean Technol, 28 (10): 1206–1227

Zou X, Zeng Z (2006). A quality control procedure for GPS radio occultation data. J Geophys Res, 111(D2): D02112